

PCCP

Accepted Manuscript



This is an *Accepted Manuscript*, which has been through the Royal Society of Chemistry peer review process and has been accepted for publication.

Accepted Manuscripts are published online shortly after acceptance, before technical editing, formatting and proof reading. Using this free service, authors can make their results available to the community, in citable form, before we publish the edited article. We will replace this *Accepted Manuscript* with the edited and formatted *Advance Article* as soon as it is available.

You can find more information about *Accepted Manuscripts* in the [Information for Authors](#).

Please note that technical editing may introduce minor changes to the text and/or graphics, which may alter content. The journal's standard [Terms & Conditions](#) and the [Ethical guidelines](#) still apply. In no event shall the Royal Society of Chemistry be held responsible for any errors or omissions in this *Accepted Manuscript* or any consequences arising from the use of any information it contains.

Surface modification of alumina-coated silica nanoparticles in aqueous sols with phosphonic acids and impact on nanoparticle interactions

Céline Schmitt Pauly^{1,2}, Anne-Caroline Genix², Johan G. Alauzun¹, Michael Sztucki³, Julian Oberdisse^{2,4}, P. Hubert Mutin¹

¹ *Institut Charles Gerhardt Montpellier, UMR 5253, CNRS-UM-ENSCM, Université de Montpellier, Place Eugène Bataillon, CC1701, F-34095 Montpellier Cedex 5, France*

² *Laboratoire Charles Coulomb (L2C), UMR 5221 CNRS-Université de Montpellier, F-34095 Montpellier, France.*

³ *ESRF - The European Synchrotron, 71 av des Martyrs, CS40220, F-38043 Grenoble, France*

⁴ *Laboratoire Léon Brillouin, UMR 12 CNRS/CEA, CEA Saclay, F-91191 Gif sur Yvette, France*

Abstract

It is often necessary to tailor nanoparticle interactions and their compatibility with a polymer matrix by grafting organic groups, but the commonly used silanization route offers little versatility in particular in water. Here, alumina-coated silica NPs in aqueous sols have been modified for the first time with low molecular-weight phosphonic acids (PAs) bearing organic groups of various hydrophobicity and charge: propyl, pentyl and octyl PAs, and two PAs bearing hydrophilic groups, either a neutral diethylene glycol (DEPA) or a potentially charged carboxylic acid group (CAPA). The interactions and aggregation in the sols have been investigated using zeta potential measurements, dynamic light scattering, transmission electron microscopy, and small-angle scattering methods. The surface modification has been studied using FTIR and ³¹P MAS NMR spectroscopies. Both high grafting density ρ and high hydrophobicity of the groups on the PA induced aggregation, whereas suspensions of NPs

grafted by DEPA remained stable up to the highest ρ . Unexpectedly, CAPA-modified NPs showed aggregation even at low ρ , suggesting that the carboxylic end group was also grafted to the surface. Surface modification of aqueous sols with PAs allows thus for the grafting of a higher density and a wider variety of organic groups than organosilanes, offering an increased control of the interactions between NPs, which is of interest for designing waterborne nanocomposites.

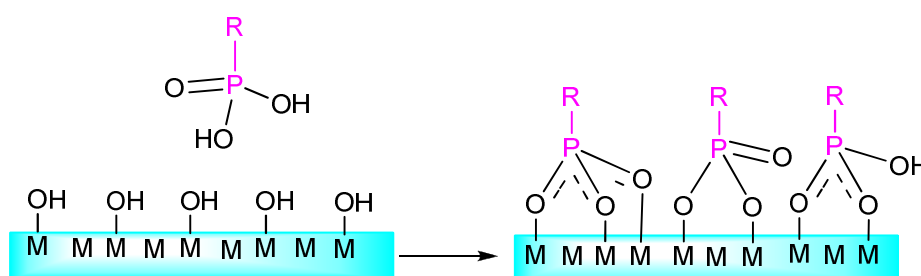
1. Introduction

Silica nanoparticles (NPs) colloids are used in numerous application areas including ceramics, composite materials, cements, catalysis, polishing, paper and textile. They are utilized for instance as adsorbents, as additives to control the rheology of formulations or induce flocculation, as binding agents in casting moulds, as fillers to improve the mechanical properties of concrete, lacquers or rubber, or as binders in catalysts and paint¹⁻³. Controlling the surface properties of silica NPs and thereby their degree of aggregation is of major fundamental and applied interest. The mechanical and optical properties of nanocomposite materials for instance directly depend on the degree of aggregation of the reinforcing NPs⁴⁻⁸ and on their compatibility with the polymer matrix⁹⁻¹¹.

Typically, aqueous silica sols are stabilized at high pH ($\sim 8 - 10$) by electrostatic repulsions between negatively charged silica particles.¹ The degree of aggregation can be controlled by playing on the pH or salt content in order to tune electrostatic repulsions.⁶ Surface functionalization by organic groups offers other possibilities to control interactions and aggregation of NPs in aqueous sols and in the final materials.^{12 13} Functionalization of silica is usually done by grafting organotrialkoxysilanes, see e.g.,¹⁴. Owing to the low solubility in water of these compounds and to their high sensitivity to hydrolysis, the surface modification is in most cases performed in organic medium to avoid anarchic polycondensation of the organotrialkoxysilanes^{15, 16}. Actually, very few studies have been reported on the surface modification of aqueous colloidal silica by organotrialkoxysilanes. Na and coworkers reported the modification of colloidal silica with methyltrimethoxysilane (MTMS) and γ -glycidoxypropyltrimethoxysilane (GPTMS). The resulting sols showed limited stability, as shown by the gradual increase of viscosity and decrease of transmittance¹⁷. Greenwood et al. found that silica sols could be efficiently grafted by slow addition of pre-hydrolyzed GPTMS.

The grafting significantly improved the hardness of waterborne resins while maintaining good optical properties^{4, 18}.

Suspensions of positively-charged silica particles stabilized at low pH (~ 4) are also commercially available¹⁹. The positive charge is due to the adsorption at the surface of the silica particles of octahedral aluminium oxo-hydroxide ions, leading to an alumina-like coating.



Scheme 1 Modification of a metal oxide surface by reaction with a phosphonic acid.

The presence of this alumina coating opens the road to surface functionalization in aqueous medium using phosphonic acids (PAs), as recently shown for aggregated silica nanoparticles (NPs)²⁰. This offers the possibility to tune the interactions (electrostatic, steric, hydrophobic...) between NPs in aqueous sols by playing with the nature of the organic group on the PA and on the grafting density. Indeed, contrary to organoalkoxysilanes, PAs are stable in aqueous solutions and do not polycondense²¹⁻²³. PAs bind to a wide range of metal oxide surfaces by formation of M-O-P bonds²⁴⁻²⁷, resulting from the condensation of P-OH groups with surface hydroxyl groups and the coordination of P=O groups to M atoms (Scheme 1)^{28, 29}. PAs cannot be used to modify pure silica surfaces in aqueous medium due to the low hydrolytic stability of Si-O-P bonds³⁰, whereas Al-O-P bonds are much more stable, hence the need for an alumina coating³¹.

There are very few publications reporting the surface modifications of metal oxide aqueous sols (CeO_2 , TiO_2) using PAs^{32,33}. Pautrot-d'Alencon et al. modified CeO_2 sols stabilized by acetate groups using 2-carboxyethylphosphonic acid, ethylphosphonic acid, and phosphonoacetic acid in order to tune the acidic character of their surface³². Rehor et al. studied the adsorption / desorption of a phosphonic acid (or a bis-phosphonic acid) bearing a lanthanide(III) complex on TiO_2 nanoparticles in colloidal suspensions stabilized by polyvinylalcohol³³.

The goal of the present article is to explore the modification of aqueous sols of alumina-coated silica stabilized by electrostatic repulsions with different phosphonic acids, and to assess the influence of this modification on interactions and colloidal stability. Five different PAs with increasing hydrophilic-lipophilic balance^{34,35} (HLB) values have been used (from 16.5 to 21.9, see Table 1), conferring decreasing hydrophobicity to the NPs: three alkylphosphonic acids with various chain lengths, and two PAs bearing hydrophilic diethylene glycol or carboxylic acid functions. This study opens the way to control first NPs aggregation in solution, and ultimately the structure of waterborne NP-polymer mixtures, like e.g. silica-latex nanocomposites^{25,36,37}.

The outline of the paper is the following. After the experimental section, the results are subdivided in two parts. First the surface modification with PAs has been characterized using elemental analysis and spectroscopic methods. Then the changes in interactions and evolution of the colloidal stability of NPs in solution have been evidenced and quantified using zetametry, dynamic light scattering (DLS), transmission electron microscopy (TEM), and small-angle X-ray (SAXS) and neutron scattering (SANS) methods.

2. Experimental section

2.1. Materials

Alumina-coated silica nanoparticles and phosphonic acids. Aqueous suspensions of silica NPs covered with an aluminium oxo-hydroxide layer (Levasil 200S/30, 30 wt%, pH 3.8, properties summarized in Table 1) were a gift from Akzo Nobel. The colloidal stability of these sols is due to electrostatic repulsion between the NPs, which are positively charged at low pH, as verified by zetametry (Table 1). The PAs used for surface modifications are n-octyl, n-pentyl and n-propyl phosphonic acid (denoted C₈PA, C₅PA, and C₃PA, respectively), 6-phosphonohexanoic acid (CAPA), and (2-(2-(2-hydroxy-ethoxy)-ethoxy)-ethyl)phosphonic acid (DEPA). C₈PA and DEPA were purchased from SiKÉMIA and CAPA from Aldrich. C₃PA and C₅PA were prepared in the laboratory (see ESI). Note that the water content of all PAs, C_{H₂O}, has been measured by thermogravimetric analysis (TGA, 12 hours isotherms), and taken into account to calculate the grafting density.

Table 1 Properties of alumina-coated silica NPs Levasil 200S/30.

Al wt % (ICP-OES)	3.9
R ^{DLS}	19 ± 1 nm σ = 0.4
R ^{TEM}	8.3 ± 2.8 nm
R (SAXS)	7.4 nm, σ = 0.38
S _{BET}	110 m ² /g
Density	2.22 g.cm ⁻³
Zeta potential at pH 4.4	55 ± 2 mV

2.2. Methods

Grafting and purification. 5 g of commercial colloidal solution was diluted by adding 10 mL of ultra-pure water and then the pH was increased up to 5 by dropwise addition of 0.1 M

NaOH. The phosphonic acid grafts were separately dissolved in 15 mL of water and the pH of the resulting solution also adjusted to 5. Both solutions were then mixed yielding a final concentration of NPs in the solution of 5 wt %, and stirred at 200 rpm at room temperature for 24 h.

For characterization by elemental analysis, and NMR and FTIR spectroscopies, the grafted NPs in the colloidal suspension were isolated by centrifugation during 20 min at 20 000 rpm, then washed twice to remove phosphonic acid in excess by centrifugation, removing the supernatant, and redispersion in water. The final wet cake was dried at room temperature under vacuum overnight. The dried NPs were grinded with mortar and pestle prior to analysis. For structural analysis in water, the pH was always fixed to 5.

The nominal grafting density ρ expressed as the number of phosphonic acid functions per unit nanoparticle surface (P/nm²) reads:

$$\rho_{\text{nom}} = \frac{m_{\text{PA}} N_{\text{A}} (1 - C_{\text{H}_2\text{O}})}{M_{\text{PA}} S_{\text{BET}} m_{\text{NPs}}} \quad (1)$$

where N_{A} is the Avogadro number, M_{PA} the molar mass of the PA, S_{BET} the specific surface area of the dried NPs, m_{PA} the mass of phosphonic acid, and m_{NPs} the one of NPs in solution. Note that ρ_{nom} is corrected for the PA water content $C_{\text{H}_2\text{O}}$. The range of nominal grafting densities studied here extends up to typically $\rho_{\text{nom}} = 5$ P/nm². The resulting real grafting density ρ measured by ICP will be given below.

Spectroscopies. Infrared (IR) and NMR measurements were used to prove the presence and state of PAs at the NPs surface. IR spectra were recorded using an Avatar 320 FT-IR spectrometer. Measurements were done in transmission mode on pellets composed of ≈ 3 mg of dried nanoparticles dispersed in 100 mg of KBr, also used for background subtraction. Solid state ³¹P Magic Angle Spinning (MAS) NMR experiments were performed on a Varian

VNMRS 400 MHz (9.4 T) spectrometer using a 3.2 mm Varian T3 HXY MAS probe. The ^{31}P chemical shift was determined using an external reference: hydroxyapatite $\text{Ca}_{10}(\text{PO}_4)_6(\text{OH})_2$ at 2.8 ppm (with respect to H_3PO_4 , 85 wt % in water).

Elemental analysis. Inductively Coupled Plasma Optical Emission Spectroscopy (ICP-OES) was used to determine Al and P contents. About 7 mg of dried NPs were mineralized by adding 1 mL of HNO_3 (70%), 1 mL of H_2SO_4 (95%), and 1 mL of HF (40%). This solution was heated for 1h30 at 170°C , then for 1 hour at 270°C on a slab in a PTFE beaker, completed with distilled water to 50 mL and injected in a Perkin Elmer Optima 2100 DV Optical Emission Spectrometer apparatus.

Zeta potential measurements. Electric surface potential measurements of NPs were done with a Zetasizer 3000 HAS after dilution of colloidal solutions with ultra-pure water to 1 wt %.

Structural analysis. Dynamic Light Scattering (DLS) is a common technique to analyze NPs with ligands.³⁸ It was used to measure apparent hydrodynamic radii R^{DLS} with a home-made set up at 90° and a wavelength of 532 nm. The data treatment is based on cumulant fits. Small-angle X-ray scattering (SAXS) was performed on beamline ID02 at the European Synchrotron Radiation Facility (ESRF, Grenoble FR) at a wavelength $\lambda = 1 \text{ \AA}$ with a sample to detector distance $D = 2.48 \text{ m}$, yielding a q -range from $3.8 \cdot 10^{-3}$ to 0.15 \AA^{-1} . Small-angle neutron scattering (SANS) was completed on beamline PACE at Laboratoire Léon Brillouin (LLB, Saclay FR) using three configurations, defined by $D = 4.7 \text{ m}$, $\lambda = 17 \text{ \AA}$; $D = 4.7 \text{ m}$, $\lambda = 5 \text{ \AA}$ and $D = 1 \text{ m}$, $\lambda = 5 \text{ \AA}$ (total q -range: $2.4 \cdot 10^{-3} - 0.35 \text{ \AA}^{-1}$). Colloidal solutions were measured in 1.5 mm thick capillaries and 1 mm Hellma cuvettes by SAXS and SANS, respectively. The scattering cross section per unit sample volume $d\Sigma/d\Omega$ (in cm^{-1}) – which we term scattered intensity $I(q)$ – was obtained by using standard procedures including

background subtraction and calibration given by ESRF and LLB. In order to enable comparison in between scattering data from different radiations, the neutron spectra have been systematically rescaled to the X-ray contrast (the NPs/water contrasts are $\Delta\rho^{\text{SAXS}} = 9.55 \cdot 10^{10} \text{ cm}^{-2}$ and $\Delta\rho^{\text{SANS}} = 4.07 \cdot 10^{10} \text{ cm}^{-2}$). Note that the rather low absolute number of aluminium atoms on each NP (see Table 1) had no influence on particle contrast.

For 3D-visualization of particle configurations compatible with our experimentally observed scattered intensities, a reverse Monte Carlo (RMC) algorithm was applied to $I(q)$ ³⁹⁻⁴². It is based on the experimental size distribution of spheres, and calculation of $I(q)$ of homogeneous interacting polydisperse spheres with excluded volume⁴³. The basic design of the algorithm is outlined in⁴⁴. The size of the cubic simulation box was set to about 1570 nm, filled to 0.2%v with ca. 2400 NPs.

Transmission Electron Microscopy (TEM) pictures were recorded with a JEOL 1200 EXII apparatus at 100 kV.

3. Results and discussion

3.1. Alumina-coated silica nanoparticles

A form factor of Levasil NPs has been measured by SAXS in dilute suspensions (0.2 vol %) and is shown in the ESI. The fit indicates that the form factor is compatible with a log-normal size distribution of NP radii ($R_0 = 7.4 \text{ nm}$, $\sigma = 0.38$, see inset). This highly polydisperse distribution was confirmed by DLS measurements, which give an apparent hydrodynamic radius of $R^{\text{DLS}} = 18.9 \text{ nm}$ and $\sigma = 0.4$. Note that the apparent hydrodynamic radius of polydisperse hard spheres can be estimated from the moments of the size distribution¹⁷

derived from SAXS, $\langle R^6 \rangle / \langle R^5 \rangle$, which gives 16.4 nm, in reasonable agreement with the DLS result. We have also estimated the average radius by TEM over 500 beads and found 8.3 nm.

The amount of aluminium oxo-hydroxide surface layer can be estimated from elemental analysis using ICP-OES and the BET specific surface area given in Table 1. The surface density of Al-atoms was found to be typically 7.9 nm^{-2} , allowing for the grafting of a dense monolayer of phosphonic acid²⁰. Zetametry gave pH-dependent zeta-potentials decreasing from 55 to 35 mV for pH values varying from 4.4 to 6.8. This positive net charge proves the presence of the alumina-like coating at the surface of the silica NPs (which would otherwise be negatively charged in this pH range) and provides electrostatic stabilization of the initial colloidal solutions.

3.2. Surface modification of NPs with phosphonic acids

The surface of NPs was modified by reaction with the phosphonic acids termed C₃PA, C₅PA, C₈PA, CAPA and DEPA. All these molecules are water-soluble at the concentrations used, which for instance is not the case for dodecyl- or octadecylphosphonic acids, discarded for this study. The pH of reaction was fixed to 5 to minimize the dissolution of surface aluminium species and precipitation of aluminium phosphonate phases^{20, 45}. The surface modification was monitored by FTIR and ³¹P solid-state NMR spectroscopies, and elemental analysis of the washed and dried NPs.

Infrared spectroscopy. The FTIR spectra of a series of NPs reacted with increasing amounts of phosphonic acid C₈PA are compared in Fig. 1(a) with the spectrum of the bare NPs. The spectra of NPs modified by the other PAs (C₃PA, C₅PA, and DEPA) are given in the ESI. In the 4000-1400 cm^{-1} range, the spectrum of the bare NPs shows a broad vibration in the 3100 to 3700 cm^{-1} range arising from O-H stretching in hydroxyl groups (Si-OH and Al-OH) and adsorbed water. The weak bands at 2010 and 1880 cm^{-1} arise from Si-O overtone and

combination modes. The presence of adsorbed water is confirmed by the deformation vibration at 1630 cm^{-1} . The spectra of the modified NPs show the presence of additional vibrations between 2800 and 3000 cm^{-1} , the intensity of which increases with the nominal grafting density. These bands correspond to the stretching of C-H bonds in the grafted phosphonate groups with the methylene symmetric and asymmetric stretching modes at 2857 and 2927 cm^{-1} , respectively, and one asymmetric stretching mode for the methyl group at 2960 cm^{-1} . The high wavenumber values observed for the C-H vibrations show that even at high grafting density the octyl chains in the monolayer are rather disordered. Below 1400 cm^{-1} , the bands arising from P-O vibrations in the $900\text{-}1200\text{ cm}^{-1}$ range^{15, 45} overlap with the intense bands due to Si-O vibrations of the bare NPs, preventing further analysis of the spectra (see Fig. S2. in ESI for the complete FTIR spectra).

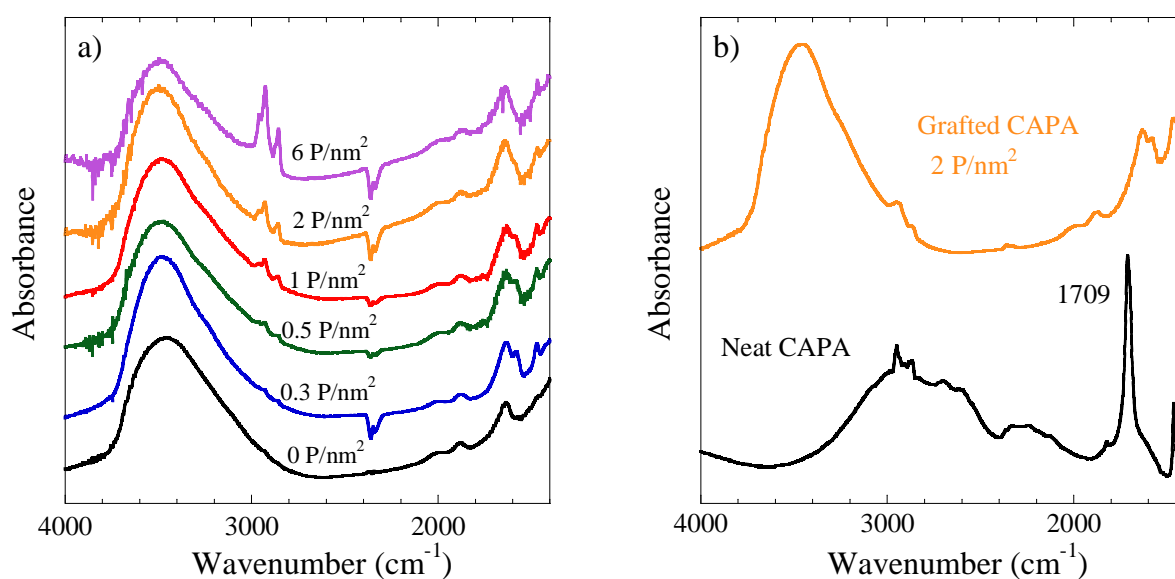
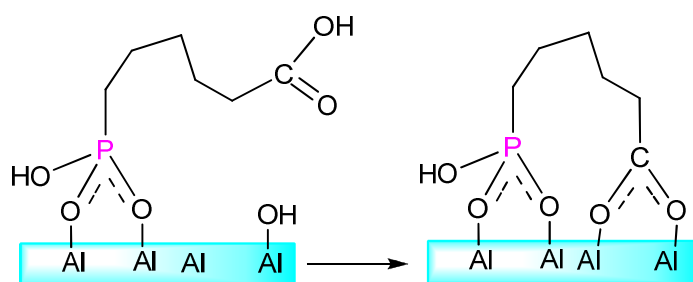


Fig. 1 (a) FTIR spectra of NPs grafted with C₈PA at nominal grafting densities between $\rho_{\text{nom}} = 0$ (bare) and 6 P/nm^2 . Spectra are normalized (see ESI) and shifted vertically for clarity. (b) FTIR spectra of pure and NPs grafted by CAPA (2 P/nm^2).

In Fig. 1(b), we have compared the spectra of CAPA and of NPs grafted with CAPA. Carboxylic acids can be used to modify alumina surfaces, although they are easily exchanged

^{46, 47}. In self-assembled monolayers formed by reaction of carboxydodecyl-phosphonic acid with a metal oxide surface, the PA groups were found to bind preferentially to the surface, leading to monolayers terminated by free carboxylic acid groups ⁴⁸. In the spectrum of grafted CAPA, the absence of the C=O stretching band at $\approx 1710\text{ cm}^{-1}$ (characteristic of the COOH group) indicates however that the carboxylate group is bonded to the NP surface as shown in Scheme 2; this situation is likely favored by the low grafting density of our monolayers.



Scheme 2 Grafting of CAPA to an alumina surface by both phosphonate and carboxylate groups.

The infrared spectra of the dried NPs are consistent with the presence of grafted phosphonate species, but the formation of an independent aluminium phosphonate phase by a dissolution-precipitation mechanism cannot be ruled out at this stage ^{20, 45}.

Nuclear magnetic resonance. ³¹P MAS-NMR allows detecting the presence of physisorbed PAs molecules or crystalline metal phosphonate phases ²⁷. However, it gives no direct information on the exact bonding modes of phosphonate species to the surface, contrary to ¹⁷O MAS-NMR ⁴⁹. The ³¹P MAS-NMR spectra of grafted NPs in Fig. 2 show in all cases broad resonances in the 0-35 ppm range. These broad signals confirm the presence of phosphonate units grafted onto the silica-alumina surface via P-O-Al bonds and also P-O-Si bonds. These P-O-Si bonds result from the condensation of P-OH groups with Si-OH groups during the drying treatment, as previously reported in the surface modification of aggregated silica-alumina NPs by octylphosphonic acid ²⁰. Note that in aqueous solution, due to the

sensitivity of P-O-Si bonds to hydrolysis³⁰ the phosphonate species should be grafted via P-O-Al bonds only.

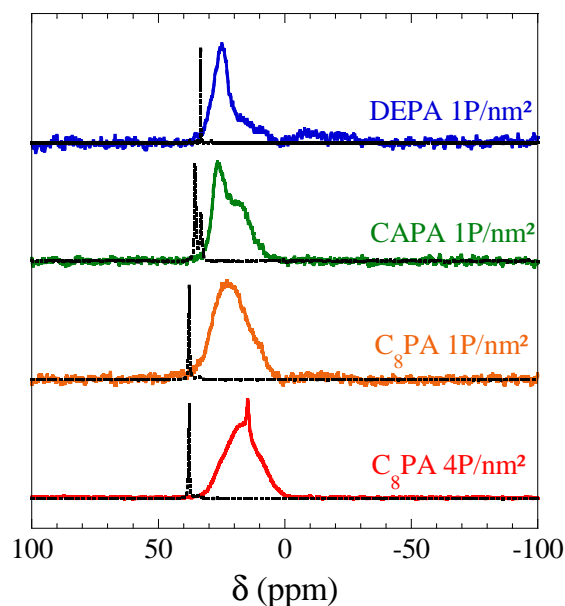


Fig. 2 ^{31}P MAS NMR of neat PAs (dotted lines) and NPs modified (solid lines) with alkylphosphonic acids C_8PA , CAPA and DEPA at nominal grafting density of 1 P/nm^2 , and at 4 P/nm^2 for C_8PA .

The absence of a sharp resonance around 30 ppm arising from free PA (see dotted lines for the neat PAs in Fig. 2 indicates that physisorbed phosphonic acid molecules were effectively removed by the washing steps. A small, sharp resonance at ca 15 ppm was detected in the spectrum of the NPs modified with $4 \text{ C}_8\text{PA/nm}^2$, indicating the minor formation of an aluminium phosphonate phase (less than 3% by integration of the spectrum) by dissolution and precipitation. In all other modified NPs, the absence of such sharp signals allows to rule out the presence of aluminium phosphonate phases.

Elemental analysis. TGA in air is commonly used to determine grafting densities in self-assembled monolayers. The TGA curves of the NPs modified by increasing amounts of C_8PA show that the weight loss between 200 and 800°C increases with the nominal grafting density (see Fig. S3 in ESI). In the same way, for a given grafting density, the weight loss increases with the molecular weight of the grafted PA (see details in ESI). This additional weight loss

corresponds to the combustion of the alkyl chains and formation of a polyphosphate residue. However, condensation of the residual hydroxyl groups also takes place in the same temperature range. This makes a precise determination of the actual grafting density difficult, particularly for low grafting densities and low molecular weight organic groups. A precise determination of the grafting density by TGA is difficult, particularly for low grafting densities and low molecular weight organic groups. The grafting density of the modified NPs was thus derived from their P content, measured using ICP-OES and from the specific surface area of the bare NPs (see ESI). In all cases we found that the data could be approximated with the following linear law, which can be seen as the low coverage part of a Langmuir isotherm:

$$\rho = 0.82 \rho_{\text{nom}} \quad (2)$$

where ρ_{nom} is the nominal grafting density. Throughout the rest of this article, the real grafting density thus determined is given. The upper limit of its error bar is estimated to $\pm 0.5 \text{ P/nm}^2$ in order to account for dispersion introduced by sample preparation and ICP measurements.

To summarize, the combination of FTIR, ^{31}P -solid state NMR, and ICP-OES results demonstrates the successful modification of the NPs by various phosphonic acids linked to the surface by P-O-M (M = Al, Si) bonds. There are no physisorbed PA molecules, and the amount of aluminium phosphonate phases is negligible. Accordingly, the P content gives a reliable estimation of the effective grafting density.

3.3. Impact of grafting on interparticle interactions

In aqueous suspension, grafting PAs on the surface of the NPs should modify the effective interactions between NPs in two ways. The first way is the decrease of the electrostatic surface charge of the NPs due to the consumption of one or two surface OH groups, to the possible presence of residual P-OH groups, and in the case of CAPA to the presence of

COOH groups. This possibility is checked by zeta potential measurements below. Secondly, for PAs carrying short alkyl chains – the length and thus hydrophobicity of which is varied here – grafting will result in a modification of the surface hydrophilicity, see Table S1 in ESI for HLB-values.

Stability. DLS, TEM, SAXS and SANS experiments have been performed at different intervals of time after grafting, from a few hours after grafting for DLS and zetametry to a few days later for small-angle scattering. It is therefore essential to characterize the evolution of the solution structure with time. This has been achieved with DLS measurements as a function of time over 6 days, for two NP concentrations, 1 wt % (as in zetametry) and 0.1 wt % (as with scattering), for various grafting densities of C₃PA and C₈PA. The results are shown in the ESI (Fig. S4). This stability study shows that there is a first stage of aggregation during grafting or immediately after, which leads to an increase of DLS radii compared to the bare NPs. The polydispersity also increases to rather high values, indicating the polydisperse character of these aggregates. The key result is that between 1 h and 6 days there is no further significant evolution with time considering the dispersion of the data. This allows direct comparison of the results of experiments on different length scales, which have necessarily been conducted after different lapses of time.

Evolution of zeta potential and aggregate size with grafting. In order to check the effect of grafting on the surface charges, the electrostatic potential of grafted NPs was evaluated at the end of the grafting reaction, using zetametry. In Fig. 3(a), the zeta-potential is seen to decrease progressively with grafting density. Up to moderate ρ (ca. 1 P/nm²), the relative impact on the surface charge is weak, within experimental error, but at high grafting density, the charge of the particles tends toward zero. Note that zeta potentials could not be measured over the whole range of grafting densities due to aggregation. The data can be divided into

two families of curves: in the case of CAPA-grafted particles, the zeta-potential decreases **faster** than with the C_n PA-family or with DEPA. Qualitatively, the decrease of the zeta-potential can be explained by the condensation of P-OH groups with surface Al-OH groups, which are at the origin of the positive charge of the particles⁵⁰. In the case of CAPA, the faster decrease of the zeta-potential can be explained by their complexation to the surface (scheme 2), which consumes additional Al-OH groups.

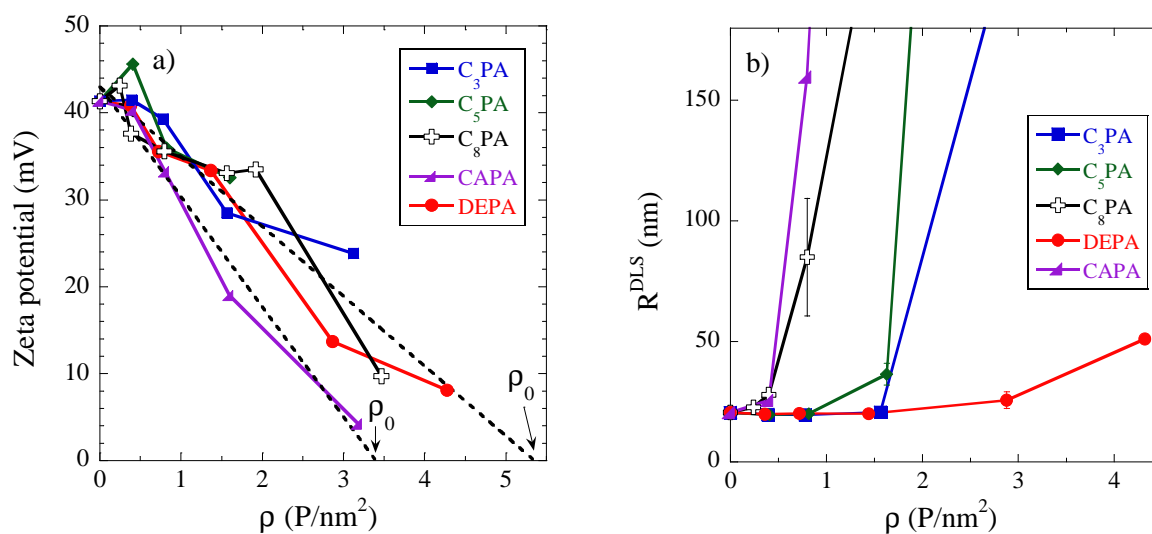


Fig. 3 (a) Zeta-potential of dilute suspensions (1 wt %, and lower for high C_8 PA grafting) of NPs in water modified with PA-molecules as indicated in the legend, as a function of the grafting density ρ at pH 5. Zeta potentials of CAPA, and of the C_n PA-family and DEPA, are compared to linear functions (dotted lines). (b) Apparent hydrodynamic radius R^{DLS} of NPs and NP-aggregates as a function of grafting density ρ .

In Fig. 3(a), we have described the zeta potentials of the C_n PA-family and DEPA, and independently those of CAPA, with linear fits leading to zero charge at a grafting density of $\rho_0 = 5.4 \pm 0.5$ P/nm² for the C_n PAs and DEPA, and 3.4 ± 0.5 P/nm² for CAPA. The ratio of these ρ_0 (or, equivalently, of the slopes) indicates that about 1.6 time more positive charges are annihilated per grafted CAPA than with the other PAs. Thus, for NPs modified by a dense alkylphosphonate monolayer (approx. 5 P/nm²) the zeta-potential is practically zero, which

suggests that all the Al-OH groups at the origin of the positive charge have been consumed by the grafting. In this case, the only possible mechanism for sol stabilization would be steric repulsion.

Unfortunately, a reliable estimation of the net charge annihilated by any phosphonic acid and/or carboxylic acid grafting is not available due to the inherent complexity of these reactions. If the alumina surface is globally positive suggesting the existence of Al-OH₂⁺ groups, many other hydroxyl groups coexist and may participate in the grafting. However, if we make the hypothesis that the zeta-potential is proportional to the number of Al-OH groups, and that all of the carboxylic acid groups of the CAPA molecules react with the surface (as suggested by the FTIR spectra in Fig. 1(b)), the ratio of the slopes gives an estimation of the average number (between 1 and 2) of P-OH/Al-OH condensations involved in the grafting of a P(O)(OH)₂ group to the surface, and of the density of Al-OH groups of the aluminium oxohydroxide layer at the surface of the raw NPs. Indeed, each carboxylic acid group condenses with one Al-OH group, and the grafting of CAPA (1 PO₃H₂ and 1 COOH group) consumes $5.4/3.4 \cong 1.6$ times more Al-OH groups than the grafting of C_nPA or DEPA (1 PO₃H₂ group). Thus, the average number of Al-OH groups consumed by the grafting of a P(O)(OH)₂ group is given by $1/(5.4/3.4-1) \cong 1.7$. This is a reasonable value, suggesting that about 85% of the P-OH groups are condensed with Al-OH groups. From this value we can deduce the starting number of Al-OH groups, which should be equal to $1.7 \times 5.4 \text{ P/nm}^2 \approx 9.2 \text{ Al-OH/nm}^2$. Again this value is reasonable: for comparison, the Al-OH density at the surface of the (0 1 0) face (the most exposed face) of γ -AlOOH is also 9.3 Al-OH/nm^2 ⁵¹.

To summarize, electrostatic repulsions decrease with ρ , leading to increased probability of collisions in suspension, and thus aggregation of NPs may be induced. The grafting density corresponding to zero charge could be estimated by extrapolation. If the charge density alone

were responsible for the NP interactions, then no significant aggregation would be expected for zeta potential higher than ≈ 20 mV, that is below ≈ 3 P/nm² for the C_nPA-family and DEPA, or below ≈ 2 P/nm² for CAPA. As we will see now, however, aggregation behavior is more subtle.

The structural evolution induced by the changes in interparticle interactions due to surface modification with PAs has been followed by DLS, which is a common method for aggregation studies^{52,53}. The results as a function of the grafting density for the different PAs are shown in Fig. 3(b). The apparent hydrodynamic aggregate radii R^{DLS} have been measured during the first day after grafting. According to Fig. 3(b), the apparent hydrodynamic aggregate radius increases first weakly with increasing grafting density, and then strongly above a critical value depending on the graft. DEPA grafting induces aggregation only at the largest ρ , and the critical grafting density decreases as follows: DEPA > C₃PA > C₅PA > C₈PA > CAPA. Confronting these results with the zetametry (Fig. 3(a)), it may be noted that the onset of aggregation for the C_nPA family is shifted to smaller grafting densities as the hydrophobicity of the graft increases, while the NP charge remains invariant. The strongest difference in aggregation behavior is observed between DEPA and CAPA grafting. In the case of the CAPA-modified NPs, aggregation starts at a surprisingly low grafting density $\rho < 1$ P/nm², considering that the carboxylic acid end group is highly hydrophilic and that the decrease of zeta potential at $\rho < 1$ P/nm² remains moderate. The fast aggregation observed for CAPA suggests that, due to the low grafting densities and relatively short alkyl chain (C₅), the carboxylate groups effectively bind to the positively charged alumina surface as discussed above for the dried particles (Fig. 1(b), Scheme 2), so that the hydrophobic methylene groups are exposed at the surface of the NPs. On the contrary, the more hydrophilic DEPA does not lead to aggregation of the NPs even up to high grafting densities.

Aggregation followed with transmission electron microscopy. In order to visualize aggregate formation, TEM of dried colloidal solutions has been used as a method of higher spatial resolution. If this technique provides qualitative evidence for aggregation, further aggregation of NPs during drying of the solutions on the TEM grids might occur. To minimize aggregation during drying, the solutions were highly diluted in ethanol down to less than 0.01 wt % of NPs, which allows drying under ambient conditions within one hour. The resulting TEM images for C₈PA-grafting are shown in Fig. 4. Note that ungrafted NPs that are well dispersed in solution stay well dispersed (Fig. 4(a)), while grafted NPs form aggregates progressively as seen in Fig. 4(b) and (c). Thus, even if the observed state (after drying) is more concentrated than the suspension, TEM images confirm the increase in aggregation with the C₈PA-grafting density.

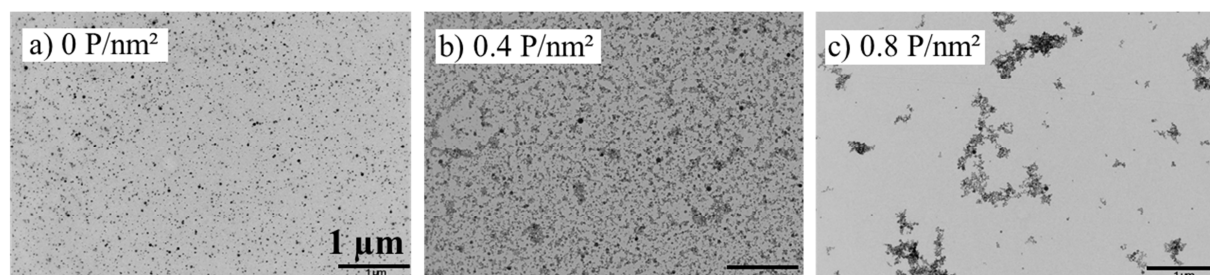


Fig. 4 TEM images showing the increase of NP-aggregation with the grafting density of C₈PA. From left to right: (a) bare NPs, (b) 0.4, and (c) 0.8 P/nm².

Changes in interactions evidenced by small-angle scattering (SAS). The problem of aggregation during drying for electron microscopy can be avoided with small-angle scattering studies directly in suspension, which gives a non destructive measurement of high spatial resolution^{54, 55}. Experiments have been carried out typically a few days after synthesis. In Fig. 5, the SAXS intensities NPs grafted with C₈PA-molecules at different densities are compared, including the bare NPs ($\rho = 0$). At the highest q , all intensities superimpose, which is due to

the identical local structure (i.e. identical NPs), and significant deviations are found only at the lowest q values, below 10^{-2} \AA^{-1} . The low- q upturns follow nicely the grafting densities, the highest ρ leading to the strongest upturn. At intermediate q , between 1 and $3 \times 10^{-2} \text{ \AA}^{-1}$, an inversion of the order of the curves is observed.

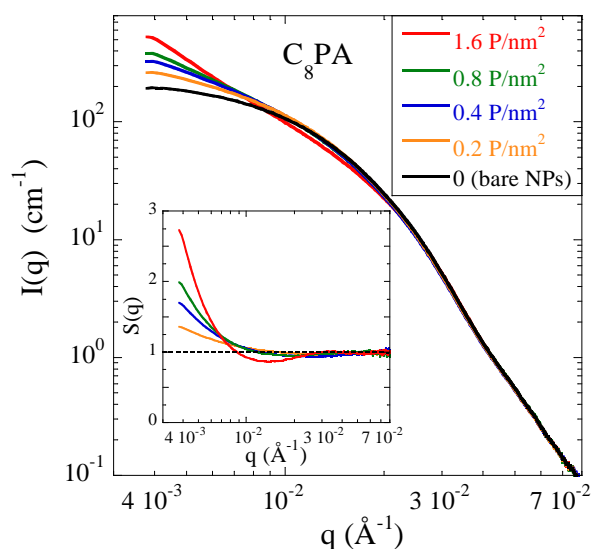


Fig. 5 SAXS scattered intensity for NPs grafted with C_8PA at 0.2 vol % in water. The grafting densities vary from 0 (bare) to 1.6 P/nm^2 . The structure factor is shown in the inset. The dotted line represents the interaction-free case ($S = 1$).

The observed behavior over the entire q -range is the signature of an aggregation process of NPs. To see this, one can determine the apparent interparticle structure factor $S(q)$, by dividing the experimental intensity $I(q)$ by the average NP form factor $P(q)$ – measured on bare NPs in Fig. 5 –, as $I(q)$ is given by:

$$I(q) = \Delta\rho^2 \Phi V P(q) S(q) \quad (3)$$

where $\Delta\rho$ is the scattering contrast, Φ the particle volume fraction, and V the individual NP volume. The resulting structure factors are shown in the inset in Fig. 5. They highlight the signature of aggregation described above, with a strong increase at low q , a moderate decrease

at intermediate q – the correlation hole –, and structure factors tending to one within error bars for higher q -values. We will focus on the low- q increase as quantitative characteristics of aggregation.

The scattered intensities in Figure 5 and the corresponding structure factor can be analyzed using a reverse Monte Carlo simulation as outlined in section 2. The result is a fit of the apparent structure factor based on the experimental size distribution given in section 3.1. Such a fit is shown in Figure 6 for the C₈PA at 1.6 P/nm². It has been obtained by positioning ca. 2400 spheres in the simulation box. For better visibility, a slice of thickness 100 nm is shown in the inset. It corresponds to a typical configuration of NPs which is compatible with the experimental structure factor. Clearly, some small aggregates, but also individual NPs, are visible in the picture. Note that contrarily to the dried TEM pictures, the NP configuration shown in the slice corresponds to the equilibrium configuration in suspension.

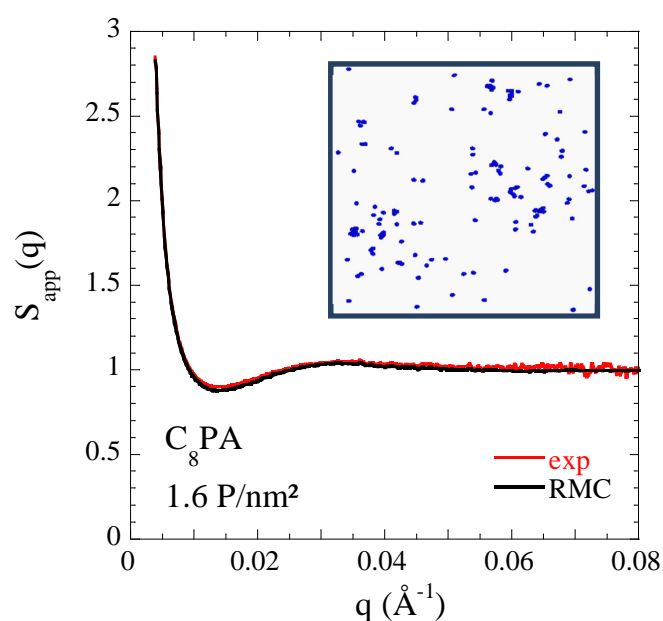


Fig. 6 RMC fit of the apparent structure factor of C₈PA-grafted NPs at 1.6 P/nm². In the inset, a 100 nm-slice of the configuration of NPs in space corresponding to the fit is shown.

The influence of grafted PAs with increasing hydrophilicity has been checked in Fig. 7, for a grafting density of $\rho = (0.8 \pm 0.5) \text{ P/nm}^2$. The scattered intensities of NPs grafted with C₅PA, C₃PA, and DEPA superimpose nicely on Fig. 7.

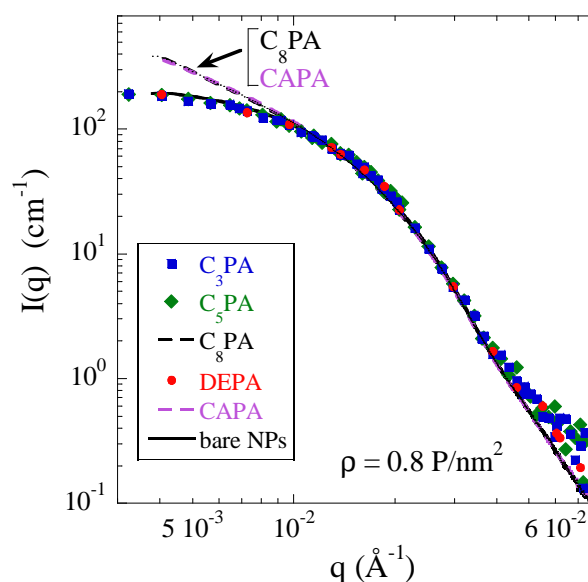


Fig. 7 Effect of grafting on NPs at 0.2 vol % in water of increasingly hydrophilic phosphonic acids C₃PA, C₅PA, C₈PA, DEPA and CAPA for a grafting density $\rho = 0.8 \text{ P/nm}^2$. The scattered intensities from SANS (symbols) were rescaled to the same contrast as the SAXS form factor (plain line).

They all coincide with the average NP form factor, which immediately gives $S(q) = 1$ for these samples according to eq 3. Grafting only $\approx 1 \text{ P/nm}^2$ of C₅PA, C₃PA, and DEPA thus does not lead to aggregation, in agreement with the DLS observations reported in Fig. 3(b). On the contrary, the results for C₈PA and CAPA at the same ρ indicate that aggregation induced by these grafts, as observed with DLS at this grafting density, is reflected by a corresponding low- q increase in SAS. The highest grafting density of 4.0 P/nm^2 for CAPA, which according to Fig. 3(b) corresponds to strongly aggregated samples, is shown in the ESI (Fig. S5).

The next step is to increase the grafting densities of the most hydrophilic PA, DEPA, to check if higher grafting densities and the corresponding decrease of electrostatic repulsion can also

trigger aggregation. The data for three grafting densities of DEPA ($\rho = 0.7, 1.4,$ and 2.9 P/nm^2) are shown in Fig. 8. Only at the highest grafting density, $\rho = 2.9 \text{ P/nm}^2$, does the low- q intensity increase (as one sees with $S(q)$ in the inset), which is the signature of aggregation. In the framework of the balance between interactions discussed above, this is interpreted as the result of the decrease of the electrostatic charges on the NP, as DEPA grafting should not increase the hydrophobicity of the NPs.

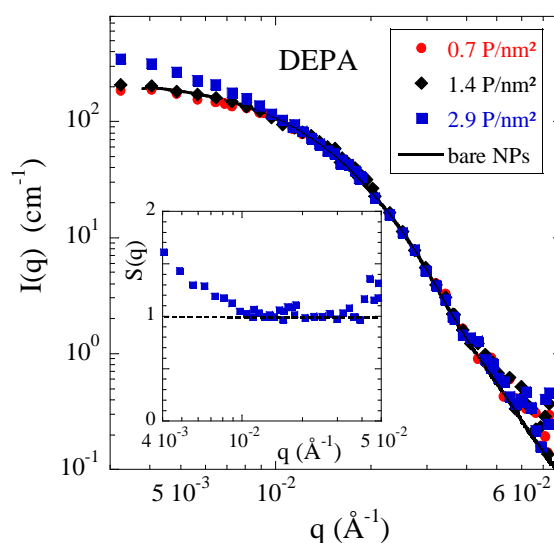


Fig. 8 Effect of grafting on NPs at 0.2 vol % in water of DEPA with grafting densities between 0 (bare) and 2.9 P/nm^2 . Inset: structure factor for NPs with 2.9 P/nm^2 . The scattered intensities from SANS (symbols) were rescaled to the same contrast as the SAXS form factor (lines).

We will now compare the influence of the different PA-grafts, as a function of the grafting density, based on the experimentally determined structure factors. The aggregates being too big to enter the available q -range, there is no low- q plateau indicative of average aggregate mass and size (e.g., via a Guinier regime) in Fig. 5 and 7. We therefore propose a measure of extent of aggregation via the strength of the upturn through the value of $S(q^*)$ taken at a common wave vector q^* . We will use $q^* = 4 \times 10^{-3} \text{ \AA}^{-1}$ allowing for comparisons between different structure factors. In Fig. 9, the values of $S(q^*)$ are reported as a function of the

grafting density for all PAs studied in this article. This figure is a convenient tool to unite all findings on changes in NP-interactions. C₃PA and C₅PA have been measured only at the lowest ρ , and together with DEPA they stay in the stable zone, below the limit arbitrarily positioned at $S(q^*) = 1.1$. From DLS in Fig. 3(b), they were found to aggregate at intermediate ρ , the more hydrophobic C₅PA making the suspension unstable before C₃PA and finally DEPA, which is indeed seen to have its low- q structure factor cross the zone boundary around 2 P/nm^2 .

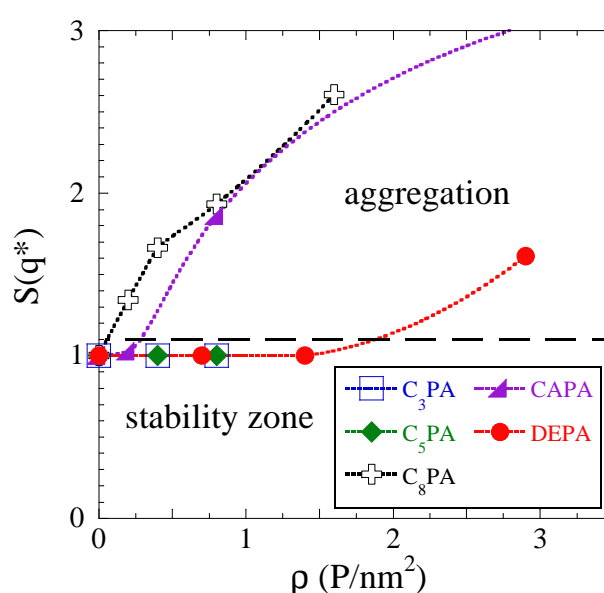


Fig. 9 Summary plot of aggregation behavior of NPs grafted with various PAs as indicated in the legend. $S(q^* = 4 \times 10^{-3} \text{ \AA}^{-1})$ represents the strength of the low- q upturn measured by small-angle scattering, as a function of the grafting density. An arbitrary limit at $S(q^*) = 1.1$ is drawn to separate the stable suspensions from those with aggregation. For CAPA, the line is continued towards the highest grafting density of 4 P/nm^2 as a guide to the eye.

The most hydrophobic C₈PA has the most pronounced low- q increase. Indeed, aggregates of intermediate radius were found by DLS already at about 1 P/nm^2 , which is reflected here by $S(q^*)$ around 2. More surprisingly, the increase of attractive interactions between NPs grafted with CAPA is less steep than with C₈PA, contrary to the DLS result. It is probable that this

reflects the dispersion in the data, and could also be due to the formation during grafting of very large aggregates which are outside the small-angle q -window. Altogether, aggregation of the NPs in suspension can be controlled by grafting well-defined amounts of PAs, C₈PA and CAPA being most effective in inducing aggregation, and DEPA on the contrary preserving stability most.

4. Conclusions

We have proposed an original method to modify the surface of alumina-coated silica NPs by organic groups *in aqueous sols*. Using phosphonic acids instead of organosilanes, sols of NPs modified by a wide range of organic groups can be prepared, with grafting densities up to 4 groups/nm² (contrary to the organosilane modification of aqueous silica sols). The impact of the grafting on the stability of the sols has been studied by zetametry, DLS, TEM, SAXS and SANS, and visualized using a RMC simulation. The grafting reaction has been characterized in detail by FTIR, NMR, and elemental analysis. To conclude on NP interactions, one may note that electrostatic stabilization and hydrophobic destabilization both evolve with the density of grafting, but differently according to the nature of the graft. The electrostatic charge of the NPs remains positive for all grafts. It was found to decrease faster with the grafting density for CAPA than for all other grafts (C_nPA-family and DEPA) due to the reactivity of the carboxylate group with the surface. For all grafts but CAPA, the electrostatic repulsions remain significant (zeta potential > 20 mV) up to grafting densities $\rho \approx 3$ P/nm², and aggregation depends on the hydrophobicity of the organic group of the PA: the higher the hydrophobicity, the lower the onset of aggregation. For grafting densities up to ca 2 P/nm², the charges remaining on the grafted NPs stabilize the suspensions for short alkyl groups only (e.g., C₃PA) and in the case of the hydrophilic DEPA. Conversely, NPs grafted by C₈PA are

aggregated even at very low grafting density and low charge reduction. This is ascribed to the grafting of the carboxylic acid group to the alumina-surface, leaving only the hydrophobic methylene groups exposed.

The surface modification of NPs in aqueous suspension opens the way to the elaboration of waterborne nanocomposites^{25, 36, 37} like, e.g., silica-latex nanocomposites, with a structural control obtained by playing on the nature and density of the organic groups. The original method of PA grafting on silica-alumina NPs in aqueous suspension presented here is an efficient and versatile method which should allow a control of aggregate formation, and thereby of rheological properties in waterborne polymer nanocomposites.

Acknowledgements: The PhD of CSP was financed by Labex ChemiSyst (ANR-10-LABX-05-01). We are indebted to Akzo Nobel for offering us their NPs, and to G. Guerrero for the gift of PAs. ESRF is acknowledged for the provision of synchrotron radiation facilities. Help by J. Jestin (LLB) and P. Gaveau (UM) with the SANS and NMR experiments is gratefully acknowledged.

Electronic Supplementary Information (ESI) available: Details regarding the synthesis of PA with short alkyl groups, the NP size, and complementary data related to IR, TGA, ICP-OES, and small-angle scattering. See DOI: 10.1039/b000000x/

References

- 1 R. K. Iler, *The Chemistry of Silica: Solubility, Polymerization, Colloid and Surface Properties and Biochemistry*, John Wiley and Son, 1979.
- 2 C. Payne, C., in *The Colloid Chemistry of Silica*, American Chemical Society, 1994, vol. 234, pp. 581-594.
- 3 H. E. Bergna, W. O. Roberts and Editors, *Colloidal Silica: Fundamentals and Applications. [In: Surfactant Sci. Ser.; 2006, 131]*, CRC Press LLC, 2006.
- 4 P. Greenwood, *JCT CoatingsTech*, 2008, **5**, 44-51.
- 5 J. T. Davies, *A quantitative kinetic theory of emulsion type I. Physical chemistry of the emulsifying agent. Gas/Liquid and Liquid/Liquid Interfaces. Proceedings of the International Congress of Surface Activity*, Butterworths, London, 1957.
- 6 M. Tatou, A.-C. Genix, A. Imaz, J. Forcada, A. Banc, R. Schweins, I. Grillo and J. Oberdisse, *Macromolecules*, 2014, **44**, 9029-9039.
- 7 N. Bosq, N. Guigo, J. Persello and N. Sbirrazzuoli, *Physical Chemistry Chemical Physics*, 2014, **16**, 7830-7840.
- 8 N. Suzuki, M. B. Zakaria, Y.-D. Chiang, K. C. W. Wu and Y. Yamauchi, *Physical Chemistry Chemical Physics*, 2012, **14**, 7427-7432.
- 9 D. Le Strat, F. Dalmas, S. Randriamahefa, J. Jestin and V. Wintgens, *Polymer*, 2013, **54**, 1466-1479.
- 10 M. Kar, M. Pauline, K. Sharma, G. Kumaraswamy and S. Sen Gupta, *Langmuir*, 2011, **27**, 12124-12133.
- 11 S. Bokern, J. Getze, S. Agarwal and A. Greiner, *Polymer*, 2011, **52**, 912-920.
- 12 R. Scotti, L. Wahba, M. Crippa, M. D'Arienzo, R. Donetti, N. Santo and F. Morazzoni, *Soft Matter*, 2012, **8**, 2131-2143.

- 13 A. P. R. Eberle, R. Castañeda-Priego, J. M. Kim and N. J. Wagner, *Langmuir*, 2012, **28**, 1866-1878.
- 14 K. W. Stöckelhuber, A. S. Svistkov, A. G. Pelevin and G. Heinrich, *Macromolecules*, 2011, **44**, 4366-4381.
- 15 P. Thissen, A. Vega, T. Peixoto and Y. J. Chabal, *Langmuir*, 2012, **28**, 17494-17505.
- 16 G. Guerrero, J. G. Alauzun, M. Granier, D. Laurencin and P. H. Mutin, *Dalton Transactions*, 2013, **42**, 12569-12585.
- 17 P. Lindner, *Neutrons, X-ray and Light Scattering (Chap. I, P.N. Pusey)*, North Holland, Elsevier, 2002.
- 18 P. Greenwood and B. Gevert, *Pigm. Resin Technol.*, 2011, **40**, 275-284.
- 19 W. O. Roberts, *Surfactant Sci. Ser.*, 2006, **131**, 131-175.
- 20 S. Lassiaz, D. Labarre, A. Galarneau, D. Brunel and P. H. Mutin, *J. Mater. Chem.*, 2011, **21**, 8199-8205.
- 21 S. H. Behrens, D. I. Christl, R. Emmerzael, P. Schurtenberger and M. Borkovec, *Langmuir*, 2000, **16**, 2566-2575.
- 22 S. Marcinko and A. Y. Fadeev, *Langmuir*, 2004, **20**, 2270-2273.
- 23 B. M. Silverman, K. A. Wieghaus and J. Schwartz, *Langmuir*, 2005, **21**, 225-228.
- 24 J. Randon, P. Blanc and R. Paterson, *Journal of Membrane Science*, 1995, **98**, 119-129.
- 25 C. Viorner, Y. Chevolut, D. Leonard, B.-O. Aronsson, P. Pechy, H. J. Mathieu, P. Descouts and M. Graetzel, *Langmuir*, 2002, **18**, 2582-2589.
- 26 S. Marcinko, R. Helmy and A. Y. Fadeev, *Langmuir*, 2003, **19**, 2752-2755.
- 27 F. Mammeri, B. Y. Le, T. J. Daou, J.-L. Gallani, S. Colis, G. Pourroy, B. Donnio, D. Guillon and S. Begin-Colin, *J. Phys. Chem. B*, 2009, **113**, 734-738.
- 28 S. H. Behrens, M. Borkovec and P. Schurtenberger, *Langmuir*, 1998, **14**, 1951-1954.

- 29 C. Queffelec, M. Petit, P. Janvier, D. A. Knight and B. Bujoli, *Chemical Reviews*, 2012, **112**, 3777-3807.
- 30 P. H. Mutin, V. Lafond, A. F. Popa, M. Granier, L. Markey and A. Dereux, *Chem. Mater.*, 2004, **16**, 5670-5675.
- 31 P. H. Mutin, G. Guerrero and A. Vioux, *J. Mater. Chem.*, 2005, **15**, 3761 - 3768.
- 32 L. Pautrot-d'Alençon, P. Barboux and J. P. Boilot, *J Sol-Gel Sci Technol*, 2006, **39**, 261-267.
- 33 I. Řehoř, V. Kubíček, J. Kotek, P. Hermann, J. Száková and I. Lukeš, *European Journal of Inorganic Chemistry*, 2011, **2011**, 1981-1989.
- 34 S. Brunauer, P. H. Emmett and E. Teller, *Journal of the American Chemical Society*, 1938, **60**, 309-319.
- 35 V. Verdinelli, P. V. Messina, P. C. Schulz and B. Vuano, *Colloids and Surfaces A: Physicochemical and Engineering Aspects*, 2008, **316**, 131-135.
- 36 E. J. W. Verwey and J. T. G. Overbeek, *Theory of the Stability of Lyophobic Colloids*, Dover Publications, 1999.
- 37 Y. Rharbi, B. Cabane, A. Vacher, M. Joanicot and F. Boue, *Europhysics Letters*, 1999, **46**, 472-478.
- 38 B. Wang, S. A. Seabrook, P. Nedumpully-Govindan, P. Chen, H. Yin, L. Waddington, V. C. Epa, D. A. Winkler, J. K. Kirby, F. Ding and P. C. Ke, *Physical Chemistry Chemical Physics*, 2015, **17**, 1728-1739.
- 39 R. L. McGreevy, *Journal of Physics: Condensed Matter*, 2001, **13**, R877.
- 40 V. Mile, O. Gereben, S. Kohara and L. Pusztai, *The Journal of Physical Chemistry B*, 2012, **116**, 9758-9767.
- 41 S. Pothoczki, L. Temleitner and L. Pusztai, *The Journal of Chemical Physics*, 2014, **140**, 054504.

- 42 J. Oberdisse, P. Hine and W. Pyckhout-Hintzen, *Soft Matter*, 2007, **3**, 476-485.
- 43 G. P. Baeza, A.-C. Genix, C. Degrandcourt, L. Petitjean, J. Gummel, M. Couty and J. Oberdisse, *Macromolecules*, 2013, **46**, 317-329.
- 44 A. Papon, H. Montes, F. Lequeux, J. Oberdisse, K. Saalwachter and L. Guy, *Soft Matter*, 2012, **8**, 4090-4096.
- 45 G. Guerrero, P. H. Mutin and A. Vioux, *J. Mater.Chem.*, 2001, **11**, 3161-3165.
- 46 D. L. Allara and R. G. Nuzzo, *Langmuir*, 1985, **1**, 45-52.
- 47 S. P. Pujari, L. Scheres, A. T. M. Marcelis and H. Zuilhof, *Angewandte Chemie International Edition*, 2014, **53**, 6322-6356.
- 48 S. Pawsey, K. Yach and L. Reven, *Langmuir*, 2002, **18**, 5205-5212.
- 49 V. Lafond, C. Gervais, J. Maquet, D. Prochnow, F. Babonneau and P. H. Mutin, *Chemistry of Materials*, 2003, **15**, 4098-4103.
- 50 A. Clavier, M. Seijo, F. Carnal and S. Stoll, *Physical Chemistry Chemical Physics*, 2015, **17**, 4346-4353.
- 51 P. Raybaud, M. Digne, R. Iftimie, W. Wellens, P. Euzen and H. Toulhoat, *Journal of Catalysis*, 2001, **201**, 236-246.
- 52 M. Kobayashi, F. Juillerat, P. Galletto, P. Bowen and M. Borkovec, *Langmuir*, 2005, **21**, 5761-5769.
- 53 G. P. Baeza, A. C. Genix, C. Degrandcourt, L. Petitjean, J. Gummel, R. Schweins, M. Couty and J. Oberdisse, *Macromolecules*, 2013, **46**, 6621-6633.
- 54 S. Mehan, V. K. Aswal and J. Kohlbrecher, *Langmuir*, 2014, **30**, 9941-9950.
- 55 M. J. Hollamby, *Physical Chemistry Chemical Physics*, 2013, **15**, 10566-10579.